Composite Peptide-Agarose Hydrogels for High-Performance 3D Immunoassays

Journal:	*ACS Applied Materials & Interfaces*
Manuscript ID	am-2021-184668.R1
Manuscript Type:	Article
Date Submitted by the Author:	25-Nov-2021
Complete List of Authors:	Bergamaschi, Greta; National Research Council, Istituto di Scienze e Tecnologie Chimiche "Giulio Natta" – National Research Council of Italy (SCITEC-CNR) Musicò, Angelo; National Research Council, Istituto di Scienze e Tecnologie Chimiche "Giulio Natta" – National Research Council of Italy (SCITEC-CNR) Frigerio, Roberto; National Research Council, Istituto di Scienze e Tecnologie Chimiche "Giulio Natta" – National Research Council of Italy (SCITEC-CNR) Strada, Alessandro; National Research Council, Istituto di Scienze e Tecnologie Chimiche "Giulio Natta" – National Research Council of Italy (SCITEC-CNR); Politecnico di Milano, Dipartimento di Chimica Materiali e Ingegneria Chimica Giulio Natta Pizzi, Andrea; Politecnico di Milano Dipartimento di Chimica Materiali e Ingegneria Chimica Giulio Natta, Talone, Benedetta; Politecnico di Milano, Physics Department Ghezzi, Jacopo; National Research Council, Istituto di Scienze e Tecnologie Chimiche "Giulio Natta" – National Research Council of Italy (SCITEC-CNR); Politecnico di Milano Gautieri, Alfonso; Politecnico di Milano, Department of Electronics, Information and Bioengineering Chiari, Marcella; National Research Council, National Research Council, Istituto di Scienze e Tecnologie Chimiche "Giulio Natta" – National Research Council of Italy (SCITEC-CNR) Metrangolo, Pierangelo; Politecnico di Milano, Chimica Materiali e Ingegneria Chimica Giulio Natta Vanna, Renzo; National Research Council, Istituto di Fotonica e Nanotecnologie - National Research Council of Italy (IFN-CNR), Baldelli Bombelli, Francesca; Politecnico di Milano, Department of Chemistry, Materials and Chemical Engineering G. Natta Cretich, Marina; National Research Council, Istituto di Scienze e Tecnologie Chimiche "Giulio Natta" – National Research Council of Italy (SCITEC-CNR) Gori, Alessandro; National Research Council, Istituto di Scienze e Tecnologie Chimiche "Giulio Natta" – National Research Council of Italy (SCITEC-CNR)

Composite Peptide-Agarose Hydrogels Towards Robust and High-Sensitivity 3D Immunoassays

Greta Bergamaschi[1§], Angelo Musicò[1§], Roberto Frigerio[1], Alessandro Strada[1,2], Andrea Pizzi[2], Benedetta Talone[3], Jacopo Ghezzi[1,4], Alfonso Gautieri[4], Marcella Chiari[1], Pierangelo Metrangolo[2], Renzo Vanna[5], Francesca Baldelli Bombelli[2], Marina Cretich[1]* and Alessandro Gori[1]*

[1]: Istituto di Scienze e Tecnologie Chimiche "Giulio Natta" – National Research Council of Italy (SCITEC-CNR), 20131 Milan (Italy)

[2]: Laboratory of Supramolecular and Bio-Nanomaterials (SBNLab), Department of Chemistry, Materials and Chemical Engineering "Giulio Natta", Politecnico di Milano, Via Luigi Mancinelli 7, 20131 Milan, Italy

[3]: Physics Department, Politecnico di Milano, P.zza Leonardo da Vinci 32, 20133 Milan, Italy

[4]: Biomolecular Engineering Lab, Dept. Electronics, Information and Bioengineering, Politecnico di Milano, 20133 Milan (Italy)

[5]: Istituto di Fotonica e Nanotecnologie - National Research Council of Italy (IFN-CNR), 20133 Milan (Italy)

[§]: these authors equally contributed

*: corresponding authors

alessandro.gori@cnr.it; marina.cretich@cnr.it

Abstract:

Canonical immunoassays rely on highly sensitive and specific capturing of circulating biomarkers by interacting biomolecular baits. In this frame, bioprobes immobilization in spatially discrete 3D spots onto analytical surfaces by hydrogel encapsulation was shown to provide relevant advantages over conventional 2D platforms. Yet, the broad application of 3D systems is still hampered by hurdles in matching their straightforward fabrication with optimal functional properties. Herein, we report on a composite hydrogel obtained by combining a self-assembling peptide (namely Q3 peptide) with low-temperature gelling agarose that proved of simple and robust application towards the fabrication of microdroplet arrays, overcoming hurdles and limitations commonly associated with 3D hydrogel assays. We demonstrate the real-case scenario feasibility of our 3D system in the profiling of Covid-19 patients sera IgG immunoreactivity, which showed remarkably improved signal-to-noise ratio over canonical assays in 2D format and exquisite specificity. Overall, the new two-components hydrogel widens the perspectives of hydrogel-based arrays and represents a step forward towards their routine use in analytical practices.

Keywords: composite hydrogels; supramolecular chemistry; microarrays; immunoassays; self-assembling peptides

Introduction

Recent years have witnessed an increasing interest in hydrogel materials as a consequence of their multifaceted application prospects that include, among others, biomaterials, drug delivery systems, and biosensing platforms.[1–3] A key figure of merit of hydrogels is their versatility: hydrogel properties can indeed be conveniently tailored and set to mimic the biological environment where biomolecular interactions occur. In this frame, a wide variety of biomolecular (e.g. polysaccharides) and synthetic (polymers, peptides) hydrogels are currently being investigated.[4,5] To further widen the space of functional properties and applications perspectives, a rising interest has recently been put on composite hydrogels (also referred to as hybrid hydrogels),[6–12] blends of distinct nanostructured (bio)materials with synergically improved properties, most often derived by favorable supramolecular interactions between the individual components.

A growing niche of hydrogels applications is the field of 3D immunoassays, where they are used as soft matrices to locally confine biomolecules onto analytical surfaces in solution-mimetic conditions. This advanced technology has been recently applied to diverse purposes, including drug screening, enzyme activity assays, miRNA detection and high-throughput assessment of biomaterials towards regenerative medicine applications.[13,14,23–28,15–22] In a broader sense, to be effective in clinical diagnostics, immunoassays must achieve low limits of detection and stringent specificity for the target biomarkers even in complex biological samples. As such, one of the biggest challenges is to set the sensitivity of analytical platforms, including ELISA and microarrays, up to a level where high sample dilution can be used, in order to minimize nonspecific interference of the sample matrix and maximize assays specificity.[29–31]

In this scenario, the efforts towards next-generation 3D immunoassays are sustained by appealing and relevant advantages over conventional planar 2D systems, such as increased loading capacity, lower non-specific binding, and enhanced signal-to-noise ratio,[32] empowering their potential analytical value (Figure 1). As a major drawback, combined features of hydrogel printability, unimpaired analytes diffusion through the matrix, and stable probes confinement are not trivial to conciliate towards straightforward 3D assays fabrication, and still represent severe obstacles to the widespread use of 3D assays.[33]

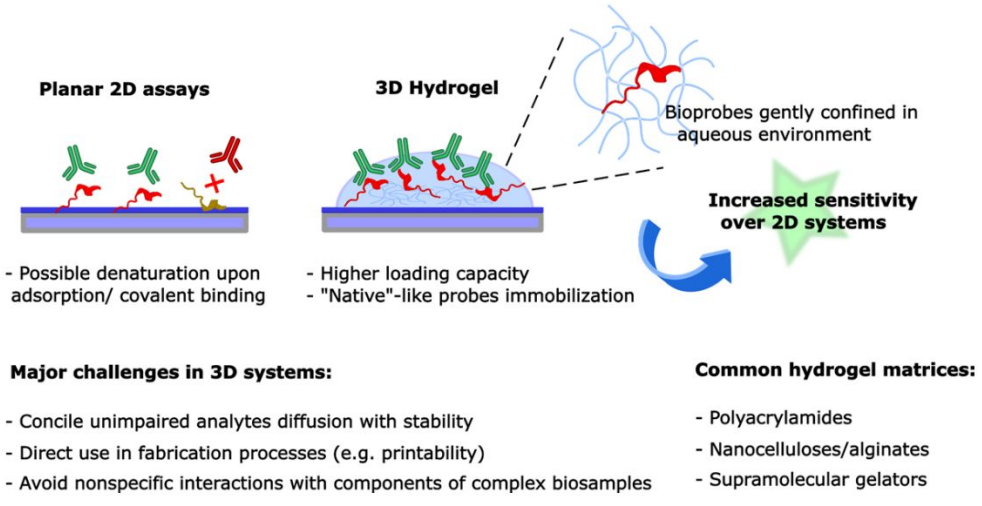

Figure 1. Comparative features of planar *vs.* 3D assays. While 2D platforms are of simple production, immobilized bioprobes can significantly suffer from surface phenomena that impair their molecular recognition properties. Conversely, 3D systems based on hydrogels are developed to preserve full functionality of confined probes, while providing increased loading capacity. On the other hand, their fabrication is not trivial.

Our group has recently contributed to this field using hydrogels based on self-assembling peptides (SAP), i.e. peptide "monomers" that spontaneously assemble into hierarchically ordered, entangled supramolecular networks with high water-holding capacity and defined viscoelastic properties.[33] The previous report, entailing the use of the YFQ11 SAP (Ac-YFQQKFQFQFEQQ-conh2), was focused on overcoming major limitations in the fabrication of 3D microarrays – mostly in enabling direct hydrogel printing, while allowing local confinement of arrayed bioprobes. Yet, assay performances were to some extent hampered by sub-optimal stability of the hydrogel droplets. Indeed, we previously reported a 10-30% loss of spotted material within the first hour of incubation, which is intrinsically a hurdle towards assays requiring prolonged incubation time (many hours to overnight) that may be needed to push the boundaries of analytical performances in the case highly diluted analytes or low affinity interactors are under study.

To tackle this limitation and further advance this field, herein we report on the use of a composite hydrogel for microarray applications obtained through the combination of a SAP, namely Q3 (sequence Ac-YFQQQFK-conh2), with low-temperature gelling agarose. In this light, we were inspired by previous reports on the favorable properties of hydrogels obtained by mixing SAP with other biopolymers.[7,8,11,34] This strategy exploits low-cost, commercially available agarose as hydrogel core structural component, while Q3 addition is crucial to balance out its rheological properties and easily introduce bio-functionalization. Besides proving stable, robust, and of straightforward application, we demonstrate that the use of the composite hydrogel in model 3D immunoassays largely outperform the conventional 2D format. Additionally, we show the superior analytical performances of 3D *vs.* planar assays in a real-case scenario by validating our platform in the profiling of Covid-19 patients sera immunoreactivity against an immunoreactive peptide epitope. Of note, our 3D system reached a discriminatory signal for Covid19-positive individuals down to 1:50000 serum dilution, which is at the operative edges of the most advanced digital detection based systems.

2. Results and discussion

2.1. Strategy design

Key hydrogel features for 3D microarrays are well-balanced properties in terms of microarray manufacturing (hydrogel printability), unimpaired biomolecules diffusion through the gel matrix and microdroplets stability in operative assay conditions, a fine balance which is non-trivial to achieve. As a result, many of the currently employed strategies for 3D systems include *in situ* hydrogel formation upon precursor solution(s) printing and cross-link.[20,24,35,36] Importantly, cross-linking often results in thick hydrogels with poor biomolecules kinetics diffusion profile or, even worse, can detrimentally affect entrapped bioprobes.

In this light, we previously relied on supramolecular peptide hydrogels that, on the other hand, may suffer of other limitations. Indeed, using the YFQ11 peptide, we experienced both a sub-optimal stability

under prolonged incubation steps and the tendence to form insoluble aggregates over time upon medium-term storage in the lyophilized powder state. In addressing these issues, we explored the possible use of composite materials with improved robustness by mixing YF-Q11 with biopolymers of common use. Indeed, the combination of SAPs with (bio)polymers of general use (*e.g.* polysaccharides, polyalcohols) affording supramolecular blends with mutually improved properties has recently been put under the spotlight as a way to expand the range of functional properties of monocomponent systems.[34,37–42] Yet, our attempts were unsuccessful, as the mixtures resulted in opalescent and aggregation-prone gels (Figure S1).

We were then prompted to investigate alternative sequences and to evaluate a small panel of YFQ11-derived peptides. This led us to identify the 7-mer sequence Ac-YFQQQFK-conh2, that we named Q3. Guiding principles for Q3 design were to use a short, amphipathic yet highly soluble peptide motif, with *N*-terminus acetylation and C-terminus polar head group as integral elements to support facile self-assembly.[43] A preliminary evaluation in terms of gelling propensity and feasibility of mixing with other components proved promising (see next paragraph).

As a counterpart, low temperature gelling agarose (hereafter referred to as Aga) was instead selected being a well-known and cheap gelling agent. While Aga can promptly form stiff hydrogels under typical usage conditions (1-1.5% w/v), these show a brittle behavior (*i.e.* low fracture point) and they lack of selective and straightforward biofunctionalization strategies. Also, of particular interest towards microarray applications, biomolecules diffusion rates through Aga gel matrix are negligible without the application of an external stimulus.[44]

In our vision, we figured that Aga gel amalgamation with the Q3 nanofibrillar network, at certain ratios, could result in a mildly viscous yet resistant gel matrix that possesses those peculiar properties required for 3D microarrays. In this strategy, SAP addition may provide the Aga hydrogel with improved physical properties, also allowing convenient functionalization with bio-reactive moieties (Figure 2).

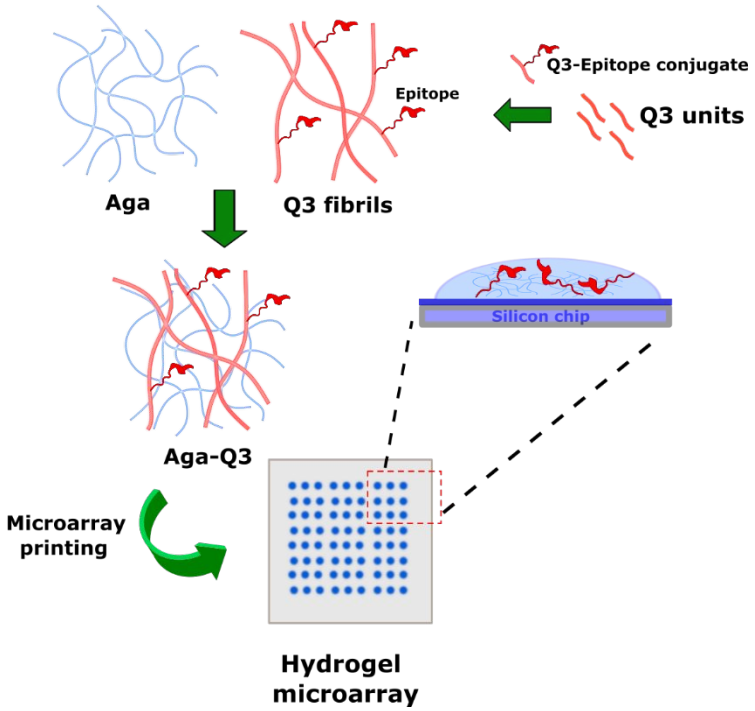

Figure 2. Conceptualized strategy used to produce 3D hydrogel arrays: i) Q3 peptide units are mixed with epitope-modified Q3 peptide to afford self-assembled functionalized Q3 fibrils; epitopes are introduced as immunoreactive probes for immunoassays ii) these are subsequently blended with agarose to yield composite hydrogels that are directly printed onto a microarray chip.

2.2. Q3 self-assembly and composite Aga-Q3 hydrogels characterization

At first, to assess self-assembling properties of Q3 peptide, 1 mM solutions were prepared in PBS buffer and overnight incubated. Transparent gels were obtained, as determined by oscillatory rheological measurements (Figure 4A). Serial dilution of Q3 solution in PBS revealed that gel-like behavior (G'>G") persisted down to 100 μM concentration. Q3 self-assembling properties were corroborated by transmission electron microscopy (TEM) experiments showing the formation of entangled nanofibrillar networks (Figure S2); remarkably peptide nanofibrils could be detected down to 25 μM concentration.

To elucidate the assembly model of Q3 peptide, molecular dynamics simulations (MD) were performed.[45,46] MD calculations highlighted the formation of beta sheets, with the most stable configuration featuring i) parallel arrangement ii) N-to C symmetry (*i.e.* antiparallel arrangement between facing beta sheets) and iii) face-to-face pairing (Figure 3 and Figure S3). These features correspond to a Class 1 steric zipper. [47] The parallel beta-sheets are stabilized by backbone hydrogen bonds (HBs), with an average distance of 4.82 ± 0.02 Å, typical of amyloid architectures. In the self-assembly of Q3, facing beta-sheets share a common interface by means of interdigitation of their side chains. Specifically, from MD simulations two different steric zipper interfaces can be distinguished, both belonging to Class 1 and featuring distances of 12.81 ± 0.14 Å and 11.84 ± 0.43 Å. Intermolecular HBs involving the self-complementary side chains stabilize the steric zipper motif. Further confirmation of the Q3 propensity to self-assemble in beta-sheets came from powder X-ray diffraction (PXRD) of freeze-dried Q3 hydrogels (Figure S4); indeed, the diffraction pattern displays a peak at $2\theta = 18.54°$ consistent with the spacing between hydrogen-bonded β-strands within β-sheets (about 4.8 Å). In addition, another peak at lower angles ($2\theta = 7.10°$) nicely correlates with the typical distances of facing β-sheets that form the well-known "steric zipper" motif (about 12 Å). Overall, these experimental data are fully coherent with MD predictions.

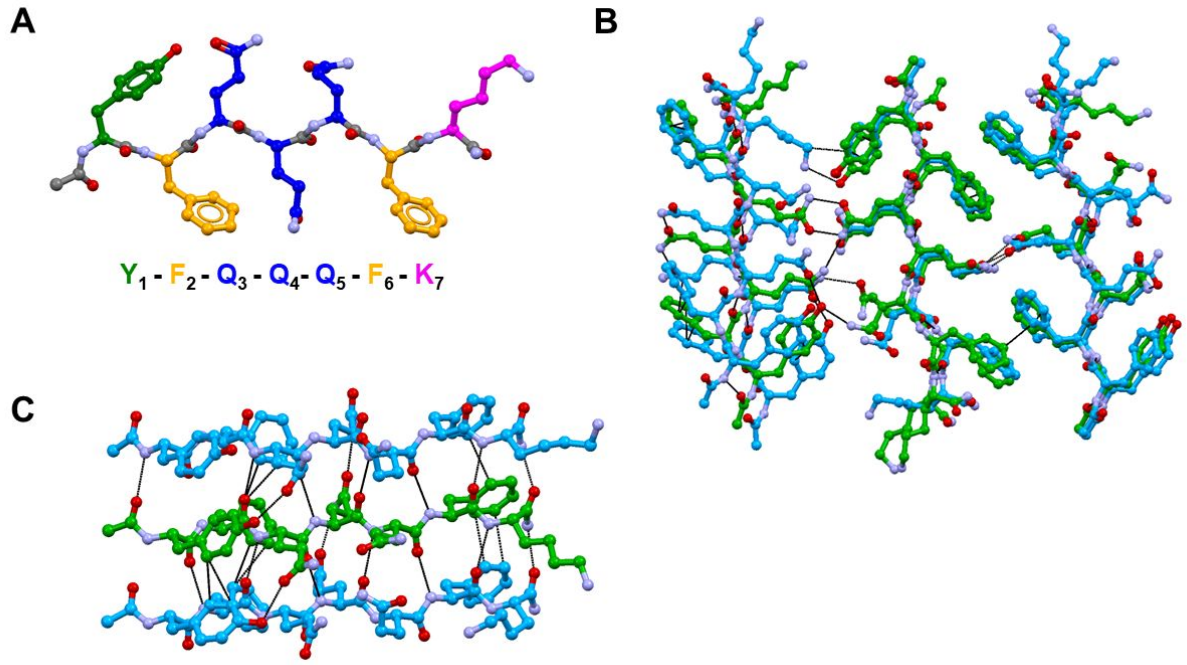

Figure 3. MD simulation of Q3. A) Linear structure of Q3 peptide (Ac-YFQQQFK-conh2); B) Q3 self-assembly, showing two distinct steric zippers; C) Highlight of a single β-sheet, consisting in the parallel stacking of Q3 strands. Intramolecular hydrogen bonds involving tyrosine and glutamines at positions 3 and 5 fix the peptide molecules in their fully extended conformation. Within the beta-sheets, in addition to the ubiquitous N-H···O contacts, a series of intermolecular HBs between glutamine residues stabilize the parallel packing. Also, a strong contribution of π- π stacking between Phe and Tyr rings further enforces this secondary structure. Hydrogen bonds and other noncovalent forces are depicted as dotted black lines. Color code: Carbon, light blue and green; oxygen, red; Nitrogen, violet. Hydrogen atoms have been omitted for clarity.

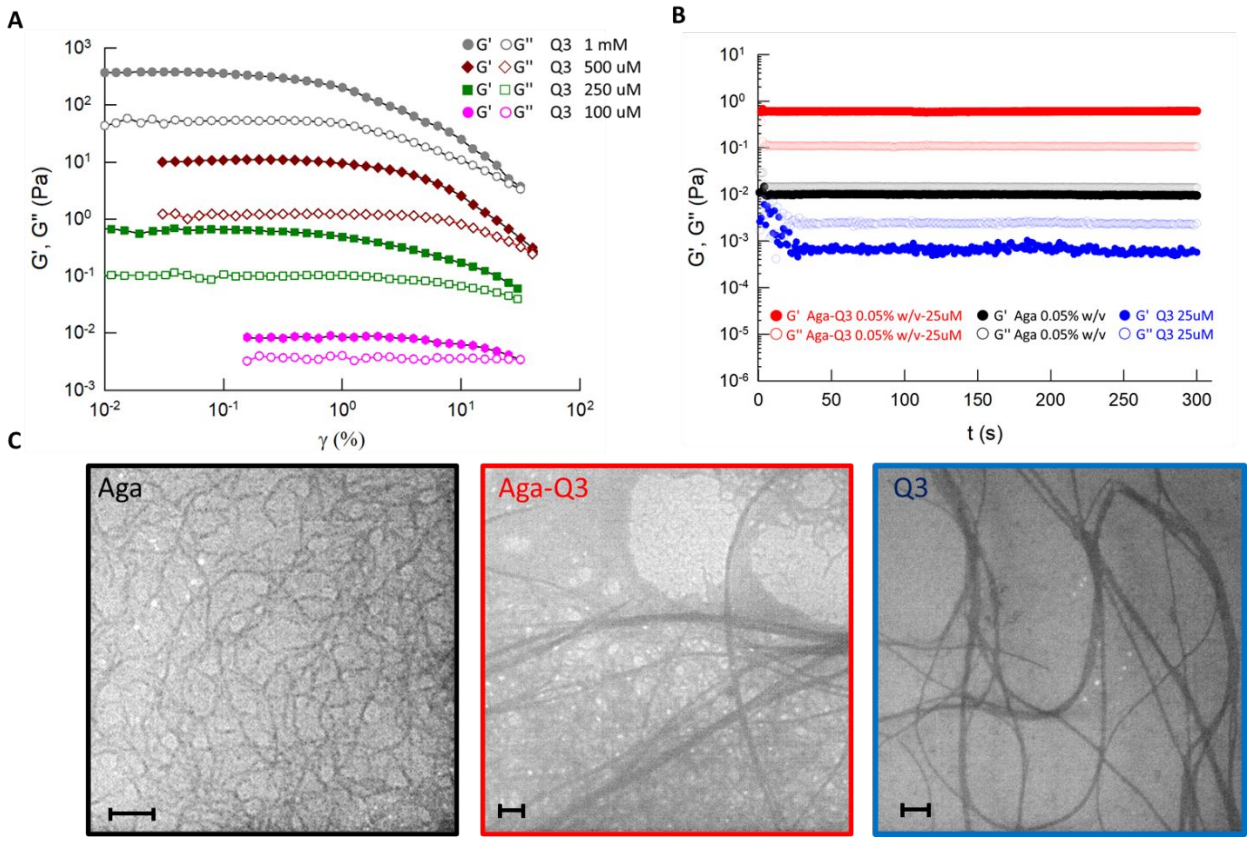

Figure 4. (A) Strain sweep experiment (Linear Visco Elastic Region) for different concentrations of Q3 in PBS. Oscillation amplitude table: frequency 0.3000 Hz, 10 samples per decade. Detailed view of the stabilizing interaction within the Q3 fibril. (B) Time sweeps experiments (0.3 Hz, 0.01 Pa) and TEM images (C) of Aga 0.05% w/v as mono-component, Aga-Q3 0.05% w/v-25μM mixture and Q3 25μM as mono-component. Scalebars correspond to 200 nm.

On these premises, we moved to probe the properties of Aga-Q3 hydrogels by mixing Q3 and Aga in variable ratios. Based on our previous findings, a G' reference value of < 10 Pa is to be considered for direct microarray printing.[33] In the case of low-gelling agarose (Aga), such a requirement is satisfied only for highly diluted (≤ 0.2% w/v) Aga solutions (Figure S4). 1 mM Q3 peptide stock aliquots were then directly diluted at different final concentrations (25-100 μM) in Aga solution (0.05-0.2% w/v) in PBS and the rheology of Aga-Q3 blends was thoroughly characterized (Figure S5). All tested samples behaved like typical viscoelastic fluids and, within the linear viscoelastic region (LVER), changes to the gel microstructures are reversibly and rapidly recovered, as shown by stress-recovery experiments (Figure S6).

Of note, we could identify a threshold in Aga concentration (0.1% w/v) above which Q3 addition weakens the hydrogel network (elastic modulus G' is lowered); on the other hand, a wider LVER is observed, along with a smoother transition out of the linear range (Figure S4), suggesting that gel blends are more tolerant to an extended deformation. Oppositely, at lower Aga concentrations (≤0.1% w/v), the blend with Q3 resulted in mutually strengthened properties, with increased G' modulus with respect to those of the monocomponent systems, suggesting a maximized and synergic interaction of the dual network of fibrils. This is particularly evident in highly diluted conditions, in which both monocomponent 25 μM Q3 and

0.05% w/v Aga revealed a fluid behavior (G" >G'), while the blended material shows predominant elastic properties (G">G', Figure 4b).

The investigation of the nanostructural features of hydrogel samples by TEM showed that Aga-Q3 blends consist in intricate fibril networks, where the two components retain their own morphological features (Figure 4c). Larger Q3 fibrils crossing through the Aga matrix, hence strengthening the overall fibril network, likely account for the enhanced rheological features of the composite hydrogel. Nanofibers distribution analysis as calculated from TEM image analysis is reported in Figure S7. Aga fibrils display a mean diameter of 16 ± 4 nm, resulting from a narrow Lorentzian curve. Q3 fibrils are larger and show higher polydispersity, with a mean diameter of 24 ± 6 nm. Of note, comparable results were obtained analyzing both samples containing the single components and the hybrid hydrogel, further confirming that the two materials retain their structural features once blended. The morphology of the supramolecular structures composing the hydrogel network was also investigated in solution by means of small angle X-ray scattering (SAXS). The scattering patterns for both Aga and Aga-Q3 were fitted using a flexible cylinder model, consistent with TEM imaging and confirming that the Aga matrix maintains its morphology even when mixed with Q3 (Figure S8).

Overall, as already described for other composite hydrogels,[48–50] it is assumed that the Aga-Q3 observed rheological behaviour is the result of electrostatic interactions as well as hydrogen bonding and hydrophobic interactions between the two separate species. While these can be very complex to finely dissect, we speculate that the interwoven Q3 fibrils could provide a scaffold for the formation of an extended supramolecular network via noncovalent interactions with the Aga network, thus resulting in a composite hydrogel with high mechanical deformability.

2.3. Set up of microarray fabrication and assay conditions by model antibody-peptide recognition test

Both Q3 and composite hydrogels were screened for the fabrication of microdroplet arrays on silicon slides coated by MCP-2,[51] a commercial polymer used to suppress non-specific background interactions in the microdroplets surroundings thanks to its anti-fouling properties. Gels rheological properties proved fully compatible with the microfluidic circuits and actuation of a non-contact piezoelectric robotic arrayer - 20 microdroplets (approximate volume 8 nL) for each spot were deposited. For composite matrices, microarray printing was feasible for Aga concentration below 0.2% w/v (8 Pa) in combination with variable Q3 amounts (25-250 μM). Upon deposition, 3D spots rapidly dried out but could be reversibly rehydrated when slides were immediately soaked into aqueous buffer (Figure 5a). Of note, monocomponent Q3 microspots showed non-reproducible stability on the chip surface upon incubation in PBS and therefore were abandoned from being further tested, while Aga-Q3 microspots were stably anchored and clearly visible even after prolonged incubation in active solution mixing (> 12 h). The 3D microspot stability was further corroborated by functional assays (see next paragraph). This feature is highly relevant since active mixing is widely used in

immunoassay protocols to accelerate the binding kinetics and avoid assay limitations in terms of analyte diffusion.

Two-photon excitated fluorescence (TPEF) microscopy experiments with fluorescein-labelled antibodies added to the hydrogel matrix prior to spotting were performed in aqueous environment to estimate the deposited microspots shape and size in wet conditions (Figure 5b). Multiple images were directly captured in water using a 1 μm pitch in the Z direction and 3D-rendering confirmed that spotted microdroplets assume a disc-like shape with a height of approximately 7 μm (8nL spot, Figure 5b).

Supported by the favorable properties shown by the Aga-Q3 blends, we designed cognate antibody-peptide recognition tests in order to optimize the experimental conditions and preliminary compare the analytical performance of 3D *vs.* 2D microarrays. As a further element of comparison, the previously introduced YFQ11-based hydrogel assay was also included in our tests using the reported optimized conditions.[33] Specifically, the immunorecognition between panflavivirus peptide epitope E01 and polyclonal rabbit antibodies (Anti-E01) spiked into human serum was used as a model interaction.[52] In 3D experimental settings, E01 epitope was immobilized within the Aga-Q3 gel matrix by means of a previously reported strategy entailing co-assembly of Q3 monomers and E01-conjugated Q3 units obtained by click chemistry,[33] which was followed by subsequent blend with Aga solutions (strategy as conceptualized in Figure 2). Optimized conditions were 25 μM Q3-E01/0.05% w/v Aga. Hydrogels were then probed with Anti-E01 antibody spiked into human serum and the interaction revealed by chemiluminescence (CL) produced by a Horse Radish Peroxidase (HRP) conjugated secondary IgG (Figure 5c). Chemiluminescence, that is enzymatically produced in wet conditions, was selected as the detection method as operating conditions could benefit more from the hydrated 3D environment.

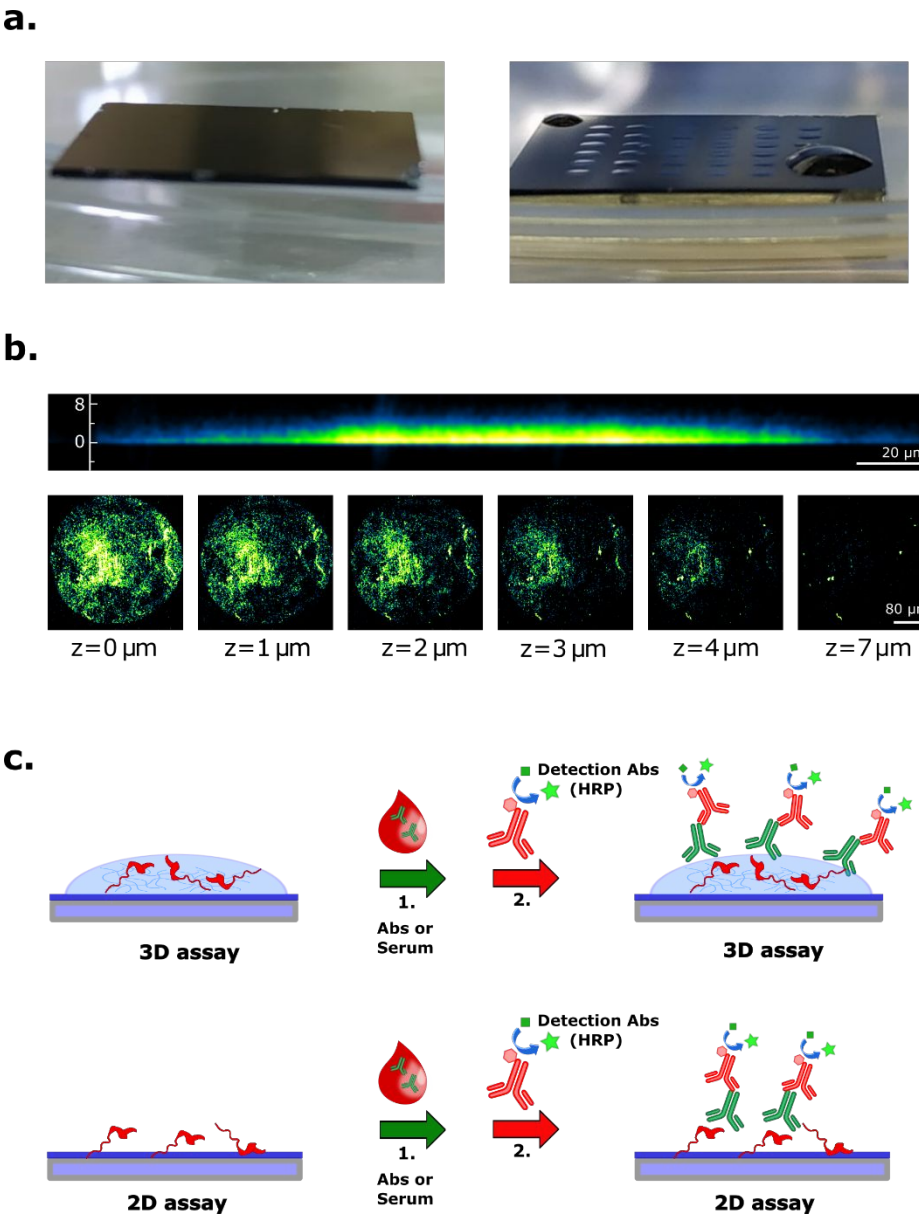

Figure 5. a) Microarray slides spotted with Aga-Q3 hydrogel in the dry (left) and wet (right) state. Regions of locally increased wettability are clearly detectable, corresponding to hydrogel spots b) TPEF images showing the average intensity projection on the sagittal (xz) plane of a 3D rendered single spotted microdroplets (top) and six 2D (xy) images collected at selected z-stack positions where z = 0µm is the optical substrate (bottom); a fluorescein tagged antibody was mixed to the preformed hydrogel prior to spotting, so that to estimate the microdroplet width and high in wet conditions c) Schematic representation of 3D and planar assays. The printed arrays are first incubated with antibodies spiked into human serum (Abs), or serum (Covid-19 test), washed and then incubated with anti IgG HRP-labelled secondary antibody for signal detection.

Several sample incubation times were tested by following the saturation curve of CL signal corresponding to the E01-Anti-E01 antibody pair (Figure 6a), which reached the 50% of maximum intensity within 2 hours and plateaued at roughly 4 hours. This lag time in the maximum intensity is likely due to the time required by the Anti-E01 antibody to thoroughly diffuse within the gel microspot. Such a protocol is

compliant with time-to-result values typical of many ELISA and microarray tests and in line with previously reported range for 3D systems.[14] Empty control spots (microdroplets lacking of the E01 epitope probe for the target) were used as a way to confirm that the hydrogel matrix is not prone to nonspecific interactions with serum components and that the detected signal arises only as a consequence of a selective molecular recognition event. Indeed, only negligible signals were detectable in empty control spots.

Subsequently, the 3D assay sensitivity was compared against equivalent assays performed in the YFQ11 configuration and in the 2D format. In the latter case, an equal (25μM) concentration of the E01 peptide was spotted directly onto the microarray surface without encapsulation in the hydrogel matrix. Spiking of Anti-E01 antibody into human serum (0 to 32 μg/mL) was then used to compare CL intensity detected for the planar 2D and 3D assays. (Figure 6b). Results clearly highlighted more favorable signal-to-noise ratio, LOD and wider detection dynamic range for the Aga-Q3 3D system. For both 3D assays, the standard curve did not reach the saturation phase at the highest applied analyte concentration of 32 μg/mL, whereas in the case of the 2D system the upper LOD was reached at 16 μg/mL. These trends suggest a favorable loading capacity proper of the 3D environment. The lower LODs for anti -E01 Ab were instead calculated by extrapolation from the linear part of the curves (Figure 6c) and are respectively 24 pM (Aga-Q3), 292 pM (2D) and 305 pM (YFQ11), which highlight an approximative 10 fold increase in sensitivity of the Aga-Q3 system for this assay with respect to the 2D format. Based on these results and other assay parameters, a comparative table with other hydrogel-based immunoassay platforms is reported in SI (see Table S2). In this sense, our proposed system matches other cutting-edge technologies, provided the variability introduced by the use of different immunoreagents and biological samples.

In this frame, it is also of note that peptides, though appealing recognition elements in terms of versatility, stability, and ease of handling, are particularly prone to suffer from detrimental interfacial effects such as loss of target recognition properties upon uncontrolled binding onto the analytical surface.[51,53,54] Traditionally, this is accompanied by limited sensitivity of peptide-based assays, hampering their widespread use. Here, we speculate that the observed superior sensitivity reached by the Aga-Q3 system could be connected the 3D geometry and to a more favorable probe-ligand interaction thanks to the minimization of non-specific ligand-surface interactions in the wet environment, resulting in a combined increased loading capacity. Indeed, in 2D systems, molecular probes properties can be altered by drying or other surface-induced effect while, in contrast, the hydrophilic environment provided by the hydrogel better preserves bioprobes integrity and function. It is also worth noticing that the similar sensitivity observed between the YFQ11 and the 2D system is likely the result of the remarkably longer incubation times applied to the 2D assay, which are instead not feasible in the YFQ11 format due to microspots instability.

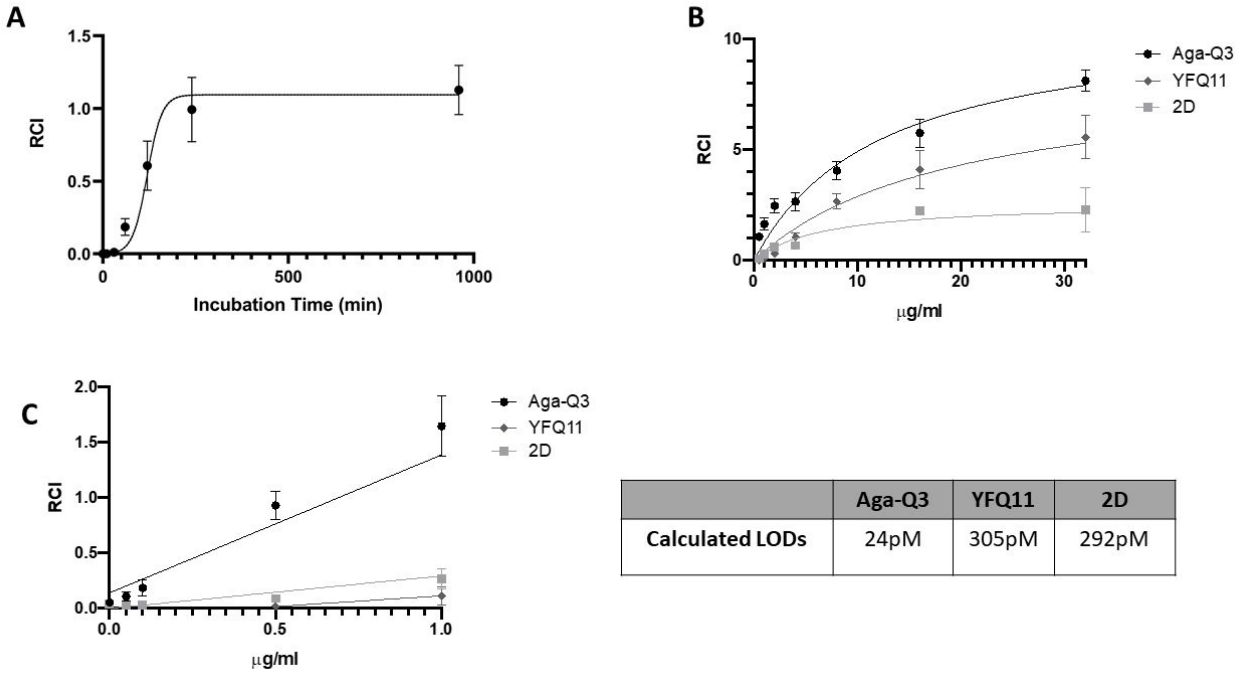

	Aga-Q3	YFQ11	2D
Calculated LODs	24pM	305pM	292pM

Figure 6. a) Saturation curve for the relative chemiluminescence intensity (RCI), showing how different sample incubation times (assay first step) reflects upon signal intensity. The maximum is reached within 4 hours of incubation and maintained even after prolonged incubation times, corroborating the stability of the 3D spots; b) Detection of different concentrations (0 -32 ug/mL) of anti-E01 antibody spiked into human serum. The chemiluminescence signals for the 2D and 3D assays are compared, showing increased signal to noise ratio and wider detection dynamic range for the 3D system; c) linear portion of curves shown in panel b were used to extrapolate the LODs for the tested systems.

2.4. 3D assays provide increased performance in SARS-CoV-2 IgG detection

We then moved to investigate the use of the selected hydrogels in a real analytical context, specifically the serological profiling in Covid-19 patients' of IgG reactivity against a peptide epitope from the SARS-CoV-2 N protein region 156-170 (hereafter named N01, sequence AIVLQLPQGTTLPKG).[55] As assay performance references, the equivalent 2D microarray format was used in order to compare similar (overnight) incubation times for the samples under analysis.

The N01 epitope was immobilized within Aga-Q3 gels by means of the same strategy previously described for E01 epitope. First, in order to estimate the ideal hydrogel probe content, decreasing amounts (from 25 μM to 1 μM) of N01 epitope within the gel matrix were tested by incubation with a set of pooled Covid-19 positive (CoV+) sera (1:1000 dilution) (Figure S9). CL signal remained unaltered down to 5 μM epitope concentration, though only a slight decrease in intensity could be observed even at 1 μM N01 content. Conversely, in the 2D assay format, the signal was almost negligible already at 10 μM. We then evaluated how the features provided by the 3D assay could be translated into sensitivity advantages by probing the detection of antibodies in highly diluted clinical samples. Thus, pooled CoV+ sera were tested at progressive dilution

and, remarkably, we could show that the 3D settings largely outperform the analogous 2D assay (Figure 7a) Indeed, while the 2D system was able to appreciate a distinctive signal only down to a 1:5.000 sera dilution (lower calculated detectable dilution factor : $9.7*10^{-4}$, Figure 7c), the 3D configuration proved approximately 10 fold more sensitive (lower calculated detectable dilution factor: $1.5*10^{-5}$, figure 7b and 7c). Overall, antibody titers could be experimentally quantified in serum in the dilution range 1:100-1:50.000 (Figure 7a). It is noteworthy that being able to operate at such samples dilution is of great advantage in terms of immunoassays specificity[31] and indicative of the ability of the assay to detect even extremely low antibody titers, often associated to mild/asymptomatic SARS-CoV-2 infections .[56]

As final validation, the immunoreactivity of two panels of serum samples (N = 12) from healthy donors (CTRL) and Covid-19 positive patients were screened against the N01 epitope in 3D format, using empty Aga-Q3 spots (without N01) as control. Upon CL detection, N01-functionalized hydrogel spots showed intense signals for all the Covid-19 positive samples whereas negligible signals were observed upon incubation with all the healthy control samples (Figure 7d), resulting in 100% sensitivity and specificity of this test. This is indicative of an effective molecular recognition of N01 epitope within the hydrogel matrix by patients' antibodies. Results of this clinical scenario were evaluated by unpaired t test, showing discrimination between the two populations at a statistically significant level ($p<0.001$), meaning that the assay is highly discriminatory (*i.e.* there is less than 1/1000 chance of error). The negligible chemiluminescence signals in the control samples suggests absence of non-specific interactions involving the hydrogel matrix. This is remarkable for complex biological samples, especially if considering the amount of potentially interfering biomolecules in human serum and complexity of immune-response in infectious diseases.

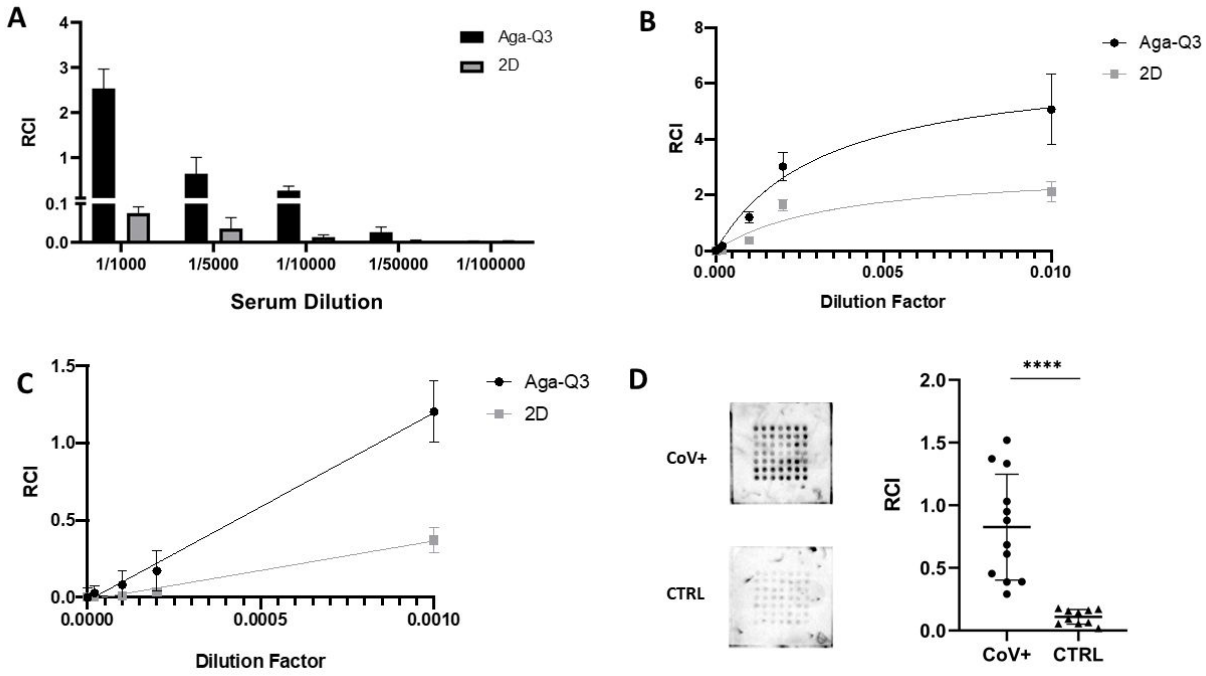

Figure 7. a) Detection of IgG reactivity against N01 peptide epitope in a pool of Covid+ patients' sera on the 2D and 3D settings. Serial dilutions of the sample were analyzed showing the capability of the 3D platform to detect a distinct CL signal down to a dilution equal to 1:50.000; b): dilution curves for the pool of Covid+ patients' sera on the 2D and 3D platforms; c) linear portion of curves shown in panel b were used to extrapolate the lower detectable dilution factors for the 2D and 3D systems; d) IgG reactivity against N01 epitope in a panel of 12 Covid+ patients' sera (CoV+) compared to that in healthy controls (CTRL). Left panel shows representative images of the array of 3D spots; right panel shows CL signals detected for the two panels. The test was able to discriminate the two populations at a statistically significant level ($p<0.0001$) with 100% specificity and sensitivity.

Conclusions

Herein we exploited a composite peptide-agarose hydrogel for developing high-performance 3D immunoassays. The two distinct hydrogel components favorably combine to provide a novel material entailing unique features towards 3D assays, as here demonstrated in microdroplet arrays fabrication. The proposed strategy indeed overcomes those limitations that impair the broad use of hydrogels for 3D immunoassays such as complex fabrication, poor biomolecules diffusion, nonspecific interactions, and overall proved user-friendly, robust and cost-effective. Importantly, the 3D assay format showed greatly superior performances with respect to conventional planar 2D assays, as here demonstrated both in model antibody-epitope recognition and in real case scenario IgG immunoreactivity profiling of Covid-19 patients. Of particular note the system allows for immunoreactivity analysis directly on complex biological matrices without affecting the molecular recognition properties of entrapped probes nor showing relevant non-specific interactions. Overall, our results consolidate the rationales driving the demand for 3D analytical platforms and represent a step forward towards new generation bioassays.

Experimental section

Peptide synthesis

A comprehensive description of all synthetic procedures is provided in the Supplementary Information section.

Hydrogel preparation

Freshly lyophilized Q3 aliquots were dissolved in PBS buffer (pH=7.4) to 1mM concentration, sonicated for 5 min and eventually diluted in PBS or agarose solution to final desired concentration and ratios. The obtained samples were then incubated at 25°C overnight and the resulting hydrogels directly used. The same procedure was used to obtain epitope functionalized hydrogels by adding freshly dissolved Q3-E01 or Q3-

N01 aliquots at desired concentration prior to overnight incubation. Same protocols for hydrogels preparation applied for the YFQ11 gels.[33]

Transmission electron microscopy

Transmission electron microscopy (TEM) images were collected using a Delong Instruments LVEM5 microscope, equipped with a field-emission gun and operating at 5 kV. Samples were prepared by placing 5 μL of hydrogels (Q3 and Ag as single component, as well as Q3-Ag mixtures) on 200 mesh carbon-coated copper grids and then removing the excess of solvent after one minute.

Hydrogel rheology

All rheology tests were performed using a KINEXUS Pro+ rheometer (MalvernPanalytical, UK). Samples were pre-formed and directly transferred on the bottom rheometer plate. The upper geometry Cone 60mm, was lowered until it was in conformal contact with the top surface of the hydrogel, corresponding to gap distances of 1.0-1.5 mm. Temperature was controlled with a Peltier device and maintained at 25°C. All the oscillatory measurements were performed within the linear viscoelastic range. Each analysis was repeated at least 3 times, and representative measures are reported.

Molecular modelling

The starting structures of Q3 fibrils are based on amyloid-like β-sheets, similar to other SAP [57–59]. The fibril models were generated using the 10 possible amyloid configurations geometries taken from Eisenberg et al. [60]. The resulting systems were characterized by 8 x 8 peptides, with an intra-sheet distance of 5 Å and an interface distance of 12 Å, according to X-ray crystals structure of similar systems [60–62]. Molecular dynamics simulations are performed following protocols used in previous studies.[45,46] Briefly, the systems were solvated in TIP3 water, resulting in systems of ≈70'000 atoms. The systems were minimized and equilibrated for 400 ps using NAMD[63]. The production run was performed for a total time of 100 ns for each configuration. The global evolution of each system was assessed by monitoring the root mean square deviation (RMSD) of peptide backbone, the root means square fluctuation (RMSF) of alpha carbons, and the native contacts. Further details are provided in the Supplementary Information.

3D Microarrays: general procedure

Silicon slides (SVM, Sunnyvail, CA) were coated with MCP2 (Lucidant Polymers) according to previous protocols[51] and hydrogels spotted using a noncontact microarray spotter (Scienion sciFLEXARRAYER S12) using an 80μM noozle, 20 droplets are deposited for each spot (approximately volume 8 nL). Spotted slides are incubated in a humid chamber for two hours before blocking with 50 mM ethanolamine in Tris/HCl 1M pH 9 for 2 hours, washed with water and dried under a stream of nitrogen. For 2D microarrays, 25μM peptide epitopes (E01 or N01) were spotted on MCP2 coated silicon slides, incubated in a humid chamber for two hours and blocked as described above.

Two-photon fluorescence microscopy

For two-photon excited fluorescence (TPEF) microscopy, hydrogel microdroplets were spotted on 0.170 mm glass coverslips. A fluorescein-labelled antibody (conc. 0.1mg/ml) was entrapped within the gel matrix prior to spotting. A home-build multimodal nonlinear microscope coupled with a mode-locked Erbium:fiber laser (FemtoFiberPro NIR, Toptica) was used.[64] The microscope works in transmission, so a couple of high magnification objectives (LD EC Epiplan-Neofluar 100x/0,75, Zeiss) is used to focus the excitation beam, at 780 nm, on the sample and to collect the two-photon fluorescent signal, then detected by a photomultiplier tube (Hamamatsu: R3896). The sample is placed on a raster scanning stage composed by a 2-axis (x-y plane) motorized translation stage (Standa: model 8MTF-102LS05), that allows to scan the sample in the focal plane, and a single-axis (z-axis) motorized translation stage (Mad City Labs Inc.: model MMP1), that allows to change the focal plane and perform z-stack acquisitions. Images of 400 x 400 μm^2 were acquired using lateral step size of 2 µm, 30 mW of laser power and 5 ms pixel dwell time. The z-stack was made by acquiring 17 different images collected at different focal planes, each at 1.0 µm distance, over a total length of 16 µm. 3D rendering image processing was performed using Fiji-ImagJ.[65]

Model Immunoassays

25µM Q3-E01/0.05% w/v Agarose for the 3D microarray, 25µM YFQ11-E01 and 25µM E01 for the 2D assay were spotted on MCP2 slides treated as described above. The resulting microarrays were incubated for 4 hours at room temperature (RT) under active mixing with Rabbit anti-E01 polyclonal antibody spiked in serum (1:100) in incubation buffer (Tris/HCl 0.05 M pH 7.6, NaCl 0.15 M, Tween 20 0.02%) with 1% w/v BSA, washed with washing buffer (Tris/HCl 0.05 M pH 9, NaCl 0.25 M, Tween 20 0.05%) for 10 minutes and incubated overnight at RT with Horse Radish Peroxidase conjugated anti-rabbit I gG (Jackson ImmunoResearch) diluted 1:1000 in incubation buffer/BSA. For the YFQ11 assay, incubation times for both steps were kept at 5 minutes as from optimized protocol[33] due to microdroplet stability reasons. After washing with washing buffer, array slides were incubated with Clarity Western ECL Substrate (Bio-Rad Hercules CA) for 2 minutes at RT to develop chemiluminescence and imaged using a Chemidoc XRS+ (Bio-Rad Hercules CA, acquisition time 21.6 seconds). Chemiluminescence intensities were corrected for spot-specific background, values for replicate spots were averaged. LOD was extrapolated using the linear regression line from the intensity value of blank samples plus three standard deviations (3σ).

Clinical immunoassays

Serum samples used in this study were leftovers from previously purchased samples[66] (Cerba Xpert, France); these both included samples collected from healthy subjects before 2018 that were used as controls and serum samples from subjects with diagnosis of SARS-CoV-2 infection. Samples were screened for immunoreactivity on Aga/Q3-N01 3D microarrays and N01 2D microarrays prepared as described above Serums were diluted 1:1000 incubation in buffer with 1% BSA and incubated over active mixing for 4 hours at RT. Slides were then washed with washing buffer, incubated with Horse Radish Peroxidase conjugated anti-human IgG (Jackson ImmunoResearch) diluted 1:1000 in incubation buffer with BSA overnight at RT.

After washing with washing buffer, array slides were incubated with chemiluminescence was detected using Clarity Western ECL Substrate (Bio-Rad Hercules CA) for 2 minutes at RT to develop chemiluminescence and imaged using a Chemidoc XRS+ (Bio-Rad Hercules CA, acquisition time 31.6 seconds). Chemiluminescence intensities were corrected for spot-specific background, values for replicate spots were averaged and data analyzed for statistical significance by GraphPad Prism 7.

Supporting Information

Additional experimental procedures and additional figures are available in the Supporting Information file.

Conflicts of Interests

The authors declare no conflict of interest.

Acknowledgements

This work was supported by the project HYDROGEX – grant n. 2018-1720, by Fondazione Cariplo and Regione Lombardia. A.G. wishes to thank Fondazione Cariplo (grant 2016-0481) and PRACE (grant COVID19-47) for funding.

References

(1) Zhou, J.; Li, J.; Du, X.; Xu, B. Supramolecular Biofunctional Materials. *Biomaterials*. Elsevier Ltd June 1, 2017, pp 1–27. https://doi.org/10.1016/j.biomaterials.2017.03.014.

(2) Prince, E.; Kumacheva, E. Design and Applications of Man-Made Biomimetic Fibrillar Hydrogels. *Nature Reviews Materials*. Nature Publishing Group February 1, 2019, pp 99–115. https://doi.org/10.1038/s41578-018-0077-9.

(3) Du, X.; Zhou, J.; Shi, J.; Xu, B. Supramolecular Hydrogelators and Hydrogels: From Soft Matter to Molecular Biomaterials. *Chem. Rev.* **2015**, *115* (24), 13165–13307. https://doi.org/10.1021/acs.chemrev.5b00299.

(4) Muir, V. G.; Burdick, J. A. Chemically Modified Biopolymers for the Formation of Biomedical Hydrogels. *Chemical Reviews*. American Chemical Society 2021. https://doi.org/10.1021/acs.chemrev.0c00923.

(5) Mondal, S.; Das, S.; Nandi, A. K. A Review on Recent Advances in Polymer and Peptide Hydrogels. *Soft Matter*. Royal Society of Chemistry February 14, 2020, pp 1404–1454. https://doi.org/10.1039/c9sm02127b.

(6) Cai, M. H.; Chen, X. Y.; Fu, L. Q.; Du, W. L.; Yang, X.; Mou, X. Z.; Hu, P. Y. Design and Development of Hybrid Hydrogels for Biomedical Applications: Recent Trends in Anticancer Drug Delivery and Tissue Engineering. *Frontiers in Bioengineering and Biotechnology*. Frontiers Media S.A. February 17, 2021, p 27. https://doi.org/10.3389/fbioe.2021.630943.

(7) Radvar, E.; Azevedo, H. S. Supramolecular Peptide/Polymer Hybrid Hydrogels for Biomedical Applications. *Macromol. Biosci.* **2019**, *19* (1), 1800221. https://doi.org/10.1002/mabi.201800221.

(8) Firipis, K.; Boyd-Moss, M.; Long, B.; Dekiwadia, C.; Hoskin, W.; Pirogova, E.; Nisbet, D. R.; Kapsa, R. M. I.; Quigley, A. F.; Williams, R. J. Tuneable Hybrid Hydrogels via Complementary Self-Assembly of a Bioactive Peptide with a Robust Polysaccharide. *ACS Biomater. Sci. Eng.* **2021**, *7* (7), 3340–3350. https://doi.org/10.1021/acsbiomaterials.1c00675.

(9) He, Y.; Abdi, M.; Trindade, G. F.; Begines, B.; Dubern, J.; Prina, E.; Hook, A. L.; Choong, G. Y. H.; Ledesma, J.; Tuck, C. J.; Rose, F. R. A. J.; Hague, R. J. M.; Roberts, C. J.; De Focatiis, D. S. A.; Ashcroft, I. A.; Williams, P.; Irvine, D. J.; Alexander, M. R.; Wildman, R. D. Exploiting Generative Design for 3D Printing of Bacterial Biofilm Resistant Composite Devices. *Adv. Sci.* **2021**, *8* (15), 2100249. https://doi.org/10.1002/advs.202100249.

(10) Chakraborty, P.; Ghosh, M.; Schnaider, L.; Adadi, N.; Ji, W.; Bychenko, D.; Dvir, T.; Adler-Abramovich, L.; Gazit, E. Composite of Peptide-Supramolecular Polymer and Covalent Polymer Comprises a New Multifunctional, Bio-Inspired Soft Material. *Macromol. Rapid Commun.* **2019**, *40* (18), 1900175. https://doi.org/10.1002/marc.201900175.

(11) Chakraborty, P.; Guterman, T.; Adadi, N.; Yadid, M.; Brosh, T.; Adler-Abramovich, L.; Dvir, T.; Gazit, E. A Self-Healing, All-Organic, Conducting, Composite Peptide Hydrogel as Pressure Sensor and Electrogenic Cell Soft Substrate. *ACS Nano* **2019**, *13* (1), 163–175. https://doi.org/10.1021/acsnano.8b05067.

(12) Wang, X.; Ronsin, O.; Gravez, B.; Farman, N.; Baumberger, T.; Jaisser, F.; Coradin, T.; Hélary, C. Nanostructured Dense Collagen-Polyester Composite Hydrogels as Amphiphilic Platforms for Drug Delivery. *Adv. Sci.* **2021**, *8* (7), 2004213. https://doi.org/10.1002/advs.202004213.

(13) Gupta, N.; Lin, B. F.; Campos, L. M.; Dimitriou, M. D.; Hikita, S. T.; Treat, N. D.; Tirrell, M. V.; Clegg, D. O.; Kramer, E. J.; Hawker, C. J. A Versatile Approach to High-Throughput Microarrays Using Thiol-Ene Chemistry. *Nat. Chem.* **2010**, *2* (2), 138–145. https://doi.org/10.1038/nchem.478.

(14) Tanase, C. P.; Albulescu, R.; Neagu, M. Application of 3D Hydrogel Microarrays in Molecular Diagnostics: Advantages and Limitations. *Expert Rev. Mol. Diagn.* **2011**, *11* (5), 461–464. https://doi.org/10.1586/erm.11.30.

(15) Koshi, Y.; Nakata, E.; Yamane, H.; Hamachi, I. A Fluorescent Lectin Array Using Supramolecular Hydrogel for Simple Detection and Pattern Profiling for Various Glycoconjugates. *J. Am. Chem. Soc.* **2006**, *128* (32), 10413–10422. https://doi.org/10.1021/ja0613963.

(16) Mateen, R.; Ali, M. M.; Hoare, T. A Printable Hydrogel Microarray for Drug Screening Avoids False Positives Associated with Promiscuous Aggregating Inhibitors. *Nat. Commun.* **2018**, *9* (1), 1–9. https://doi.org/10.1038/s41467-018-02956-z.

(17) Lorson, T.; Jaksch, S.; Lübtow, M. M.; Jüngst, T.; Groll, J.; Lühmann, T.; Luxenhofer, R. A Thermogelling Supramolecular Hydrogel with Sponge-Like Morphology as a Cytocompatible Bioink. *Biomacromolecules* **2017**, *18* (7), 2161–2171. https://doi.org/10.1021/acs.biomac.7b00481.

(18) Wang, Q.; Li, L.; Xu, B. Bioinspired Supramolecular Confinement of Luminol and Heme Proteins to Enhance the Chemiluminescent Quantum Yield. *Chem. - A Eur. J.* **2009**, *15* (13), 3168–3172. https://doi.org/10.1002/chem.200801653.

(19) Datar, A.; Joshi, P.; Lee, M. Y. Biocompatible Hydrogels for Microarray Cell Printing and Encapsulation. *Biosensors* **2015**, *5* (4), 647–663. https://doi.org/10.3390/bios5040647.

(20) Li, H.; Leulmi, R. F.; Juncker, D. Hydrogel Droplet Microarrays with Trapped Antibody-Functionalized Beads for Multiplexed Protein Analysis. *Lab Chip* **2011**, *11* (3), 528–534. https://doi.org/10.1039/c0lc00291g.

(21) Lian, M.; Chen, X.; Lu, Y.; Yang, W. Self-Assembled Peptide Hydrogel as a Smart Biointerface for Enzyme-Based Electrochemical Biosensing and Cell Monitoring. *ACS Appl. Mater. Interfaces* **2016**, *8* (38), 25036–25042. https://doi.org/10.1021/acsami.6b05409.

(22) Kiyonaka, S.; Sada, K.; Yoshimura, I.; Shinkai, S.; Kato, N.; Hamachi, I. Semi-Wet Peptide/Protein Array Using Supramolecular Hydrogel. *Nat. Mater.* **2004**, *3* (1), 58–64. https://doi.org/10.1038/nmat1034.

(23) Ikeda, M.; Ochi, R.; Hamachi, I. Supramolecular Hydrogel-Based Protein and Chemosensor Array. *Lab Chip* **2010**, *10* (24), 3325–3334. https://doi.org/10.1039/c004908e.

(24) Dong, X. H.; Obermeyer, A. C.; Olsen, B. D. Three-Dimensional Ordered Antibody Arrays Through Self-Assembly of Antibody–Polymer Conjugates. *Angew. Chemie - Int. Ed.* **2017**, *56* (5), 1273–1277. https://doi.org/10.1002/anie.201607085.

(25) Rocca, M.; Dufresne, M.; Salva, M.; Niemeyer, C. M.; Delamarche, E. Microscale Interfacial Polymerization on a Chip. *Angew. Chemie Int. Ed.* **2021**, *60* (45), 24064–24069. https://doi.org/10.1002/anie.202110974.

(26) Zhao, C.; Hou, J.; Chen, R.; Xin, Z.; Shi, H.; Wong, S. C.; Yin, J.; Shi, Q. Cell-Inspired Biointerfaces Constructed from Patterned Smart Hydrogels for Immunoassays in Whole Blood. *J. Mater. Chem. B* **2017**, *5* (12), 2315–2321. https://doi.org/10.1039/c6tb03385g.

(27) Herrmann, A.; Kaufmann, L.; Dey, P.; Haag, R.; Schedler, U. Bioorthogonal in Situ Hydrogels Based on Polyether Polyols for New Biosensor Materials with High Sensitivity. *ACS Appl. Mater. Interfaces* **2018**, *10* (13), 11382–11390. https://doi.org/10.1021/acsami.8b01860.

(28) Stumpf, A.; Brandstetter, T.; Hübner, J.; Rühe, J. Hydrogel Based Protein Biochip for Parallel Detection of Biomarkers for Diagnosis of a Systemic Inflammatory Response Syndrome (SIRS) in Human Serum. *PLoS One* **2019**, *14* (12), e0225525. https://doi.org/10.1371/journal.pone.0225525.

(29) Johansson, M. A.; Hellenäs, K. E. Matrix Effects in Immunobiosensor Determination of Clenbuterol in Urine and Serum. *Analyst* **2004**, *129* (5), 438–442. https://doi.org/10.1039/b316723b.

(30) Rosenberg-Hasson, Y.; Hansmann, L.; Liedtke, M.; Herschmann, I.; Maecker, H. T. Effects of Serum and Plasma Matrices on Multiplex Immunoassays. *Immunol. Res.* **2014**, *58* (2–3), 224–233. https://doi.org/10.1007/s12026-014-8491-6.

(31) Selby, C. Interference in Immunoassay. *Annals of Clinical Biochemistry*. Royal Society of Medicine Press Ltd November 29, 1999, pp 704–721. https://doi.org/10.1177/000456329903600603.

(32) Solin, K.; Beaumont, M.; Rosenfeldt, S.; Orelma, H.; Borghei, M.; Bacher, M.; Opietnik, M.; Rojas, O. J. Self-Assembly of Soft Cellulose Nanospheres into Colloidal Gel Layers with Enhanced Protein Adsorption Capability for Next-Generation Immunoassays. *Small* **2020**, *16* (50), 2004702. https://doi.org/10.1002/smll.202004702.

(33) Gagni, P.; Romanato, A.; Bergamaschi, G.; Bettotti, P.; Vanna, R.; Piotto, C.; Morasso, C. F.; Chiari, M.; Cretich, M.; Gori, A. A Self-Assembling Peptide Hydrogel for Ultrarapid 3D Bioassays. *Nanoscale Adv.* **2019**, *1* (2), 490–497. https://doi.org/10.1039/c8na00158h.

(34) Huang, R.; Qi, W.; Feng, L.; Su, R.; He, Z. Self-Assembling Peptide-Polysaccharide Hybrid Hydrogel as a Potential Carrier for Drug Delivery. *Soft Matter* **2011**, *7* (13), 6222–6230. https://doi.org/10.1039/c1sm05375b.

(35) Moschallski, M.; Evers, A.; Brandstetter, T.; Rühe, J. Sensitivity of Microarray Based Immunoassays Using Surface-Attached Hydrogels. *Anal. Chim. Acta* **2013**, *781*, 72–79. https://doi.org/10.1016/j.aca.2013.04.013.

(36) Sugaya, S.; Kakegawa, S.; Fukushima, S.; Yamada, M.; Seki, M. Micropatterning of Hydrogels on Locally Hydrophilized Regions on Pdms by Stepwise Solution Dipping and in Situ Gelation. *Langmuir* **2012**, *28* (39), 14073–14080. https://doi.org/10.1021/la3014706.

(37) Cornwell, D. J.; Okesola, B. O.; Smith, D. K. Hybrid Polymer and Low Molecular Weight Gels-Dynamic Two-Component Soft Materials with Both Responsive and Robust Nanoscale Networks. *Soft Matter* **2013**, *9* (36), 8730–8736. https://doi.org/10.1039/c3sm51967h.

(38) Das Mahapatra, R.; Dey, J.; Weiss, R. G. Poly(Vinyl Alcohol)-Induced Thixotropy of an L-Carnosine-Based Cytocompatible, Tripeptidic Hydrogel. *Soft Matter* **2019**, *15* (3), 433–441. https://doi.org/10.1039/c8sm01766b.

(39) Vieira, V. M. P.; Hay, L. L.; Smith, D. K. Multi-Component Hybrid Hydrogels-Understanding the Extent of Orthogonal Assembly and Its Impact on Controlled Release. *Chem. Sci.* **2017**, *8* (10), 6981–

6990. https://doi.org/10.1039/c7sc03301j.

(40) Radvar, E.; Azevedo, H. S. Supramolecular Peptide/Polymer Hybrid Hydrogels for Biomedical Applications. *Macromol. Biosci.* **2019**, *19* (1), 1800221. https://doi.org/10.1002/mabi.201800221.

(41) Cornwell, D. J.; Smith, D. K. Expanding the Scope of Gels - Combining Polymers with Low-Molecular-Weight Gelators to Yield Modified Self-Assembling Smart Materials with High-Tech Applications. *Materials Horizons*. Royal Society of Chemistry May 1, 2015, pp 279–293. https://doi.org/10.1039/c4mh00245h.

(42) Wang, J.; Wang, Z.; Gao, J.; Wang, L.; Yang, Z.; Kong, D.; Yang, Z. Incorporation of Supramolecular Hydrogels into Agarose Hydrogels - A Potential Drug Delivery Carrier. *J. Mater. Chem.* **2009**, *19* (42), 7892–7896. https://doi.org/10.1039/b913158b.

(43) Hauser, C. A. E.; Deng, R.; Mishra, A.; Loo, Y.; Khoe, U.; Zhuang, F.; Cheong, D. W.; Accardo, A.; Sullivan, M. B.; Riekel, C.; Ying, J. Y.; Hauser, U. A. Natural Tri- to Hexapeptides Self-Assemble in Water to Amyloid β-Type Fiber Aggregates by Unexpected α-Helical Intermediate Structures. *Proc. Natl. Acad. Sci. U. S. A.* **2011**, *108* (4), 1361–1366. https://doi.org/10.1073/pnas.1014796108.

(44) Weinberger, R. Size Separations in Capillary Gels and Polymer Networks. In *Practical Capillary Electrophoresis*; Elsevier, 2000; pp 245–292. https://doi.org/10.1016/b978-012742356-2/50008-0.

(45) Gautieri, A.; Beeg, M.; Gobbi, M.; Rigoldi, F.; Colombo, L.; Salmona, M. The Anti-Amyloidogenic Action of Doxycycline: A Molecular Dynamics Study on the Interaction with Aβ42. *Int. J. Mol. Sci.* **2019**, *20* (18), 4641. https://doi.org/10.3390/ijms20184641.

(46) Rigoldi, F.; Metrangolo, P.; Redaelli, A.; Gautieri, A. Nanostructure and Stability of Calcitonin Amyloids. *J. Biol. Chem.* **2017**, *292* (18), 7348–7357. https://doi.org/10.1074/jbc.M116.770271.

(47) Sawaya, M. R.; Sambashivan, S.; Nelson, R.; Ivanova, M. I.; Sievers, S. A.; Apostol, M. I.; Thompson, M. J.; Balbirnie, M.; Wiltzius, J. J. W.; McFarlane, H. T.; Madsen, A.; Riekel, C.; Eisenberg, D. Atomic Structures of Amyloid Cross-β Spines Reveal Varied Steric Zippers. *Nature* **2007**, *447* (7143), 453–457. https://doi.org/10.1038/nature05695.

(48) Yang, Z.; Chaieb, S.; Hemar, Y.; De Campo, L.; Rehm, C.; McGillivray, D. J. Investigating Linear and Nonlinear Viscoelastic Behaviour and Microstructures of Gelatin-Multiwalled Carbon Nanotube Composites. *RSC Adv.* **2015**, *5* (130), 107916–107926. https://doi.org/10.1039/c5ra22744e.

(49) Afghah, F.; Altunbek, M.; Dikyol, C.; Koc, B. Preparation and Characterization of Nanoclay-Hydrogel Composite Support-Bath for Bioprinting of Complex Structures. *Sci. Rep.* **2020**, *10* (1), 1–13. https://doi.org/10.1038/s41598-020-61606-x.

(50) Chowdhuri, S.; Ghosh, M.; Adler-Abramovich, L.; Das, D. The Effects of a Short Self-Assembling Peptide on the Physical and Biological Properties of Biopolymer Hydrogels. *Pharmaceutics* **2021**, *13* (10), 1602. https://doi.org/10.3390/pharmaceutics13101602.

(51) Gori, A.; Sola, L.; Gagni, P.; Bruni, G.; Liprino, M.; Peri, C.; Colombo, G.; Cretich, M.; Chiari, M. Screening Complex Biological Samples with Peptide Microarrays: The Favorable Impact of Probe Orientation via Chemoselective Immobilization Strategies on Clickable Polymeric Coatings. *Bioconjug. Chem.* **2016**, *27* (11), 2669–2677. https://doi.org/10.1021/acs.bioconjchem.6b00426.

(52) Bergamaschi, G.; Fassi, E. M. A.; Romanato, A.; D'Annessa, I.; Odinolfi, M. T.; Brambilla, D.; Damin, F.; Chiari, M.; Gori, A.; Colombo, G.; Cretich, M. Computational Analysis of Dengue Virus Envelope Protein (E) Reveals an Epitope with Flavivirus Immunodiagnostic Potential in Peptide Microarrays. *Int. J. Mol. Sci.* **2019**, *20* (8), 1921. https://doi.org/10.3390/ijms20081921.

(53) Gori, A.; Cretich, M.; Vanna, R.; Sola, L.; Gagni, P.; Bruni, G.; Liprino, M.; Gramatica, F.; Burastero, S.; Chiari, M. Multiple Epitope Presentation and Surface Density Control Enabled by Chemoselective Immobilization Lead to Enhanced Performance in IgE-Binding Fingerprinting on Peptide Microarrays. *Anal. Chim. Acta* **2017**, *983*, 189–197. https://doi.org/10.1016/j.aca.2017.06.027.

(54) Gori, A.; Romanato, A.; Greta, B.; Strada, A.; Gagni, P.; Frigerio, R.; Brambilla, D.; Vago, R.; Galbiati, S.; Picciolini, S.; Bedoni, M.; Daaboul, G. G.; Chiari, M.; Cretich, M. Membrane-Binding Peptides for Extracellular Vesicles on-Chip Analysis. *J. Extracell. Vesicles* **2020**, *9* (1), 1751428. https://doi.org/10.1080/20013078.2020.1751428.

(55) Musicò, A.; Frigerio, R.; Mussida, A.; Barzon, L.; Sinigaglia, A.; Riccetti, S.; Gobbi, F.; Piubelli, C.; Bergamaschi, G.; Chiari, M.; Gori, A.; Cretich, M. SARS-CoV-2 Epitope Mapping on Microarrays Highlights Strong Immune-Response to N Protein Region. *Vaccines* **2021**, *9* (1), 35. https://doi.org/10.3390/vaccines9010035.

(56) Nilsson, A. C.; Holm, D. K.; Justesen, U. S.; Gorm-Jensen, T.; Andersen, N. S.; Øvrehus, A.; Johansen, I. S.; Michelsen, J.; Sprogøe, U.; Lillevang, S. T. Comparison of Six Commercially Available SARS-CoV-2 Antibody Assays—Choice of Assay Depends on Intended Use. *Int. J. Infect. Dis.* **2021**, *103*, 381–388. https://doi.org/10.1016/j.ijid.2020.12.017.

(57) Gautieri, A.; Milani, A.; Pizzi, A.; Rigoldi, F.; Redaelli, A.; Metrangolo, P. Molecular Dynamics Investigation of Halogenated Amyloidogenic Peptides. *J. Mol. Model.* **2019**, *25* (5). https://doi.org/10.1007/s00894-019-4012-9.

(58) Rigoldi, F.; Metrangolo, P.; Redaelli, A.; Gautieri, A. Nanostructure and Stability of Calcitonin Amyloids. *J. Biol. Chem.* **2017**, *292*, jbc.M116.770271. https://doi.org/10.1074/jbc.M116.770271.

(59) Colombo, G.; Morra, G.; Pizzi, A.; Meli, M.; Gazzera, L.; Metrangolo, P.; Terraneo, G.; Genoni, A.; Bertolani, A.; Pirrie, L.; Cavallo, G. Crystal Structure of the DFNKF Segment of Human Calcitonin Unveils Aromatic Interactions between Phenylalanines. *Chem. - A Eur. J.* **2016**, *23* (9), 2051–2058. https://doi.org/10.1002/chem.201604639.

(60) Eisenberg, D. S.; Sawaya, M. R. Structural Studies of Amyloid Proteins at the Molecular Level. *Annu. Rev. Biochem.* **2017**, *86* (1), 69–95. https://doi.org/10.1146/annurev-biochem-061516-045104.

(61) Sawaya, M. R.; Sambashivan, S.; Nelson, R.; Ivanova, M. I.; Sievers, S. A.; Apostol, M. I.; Thompson, M. J.; Balbirnie, M.; Wiltzius, J. J. W.; McFarlane, H. T.; Madsen, A.; Riekel, C.; Eisenberg, D. Atomic Structures of Amyloid Cross-β Spines Reveal Varied Steric Zippers. *Nature* **2007**, *447* (7143), 453–457. https://doi.org/10.1038/nature05695.

(62) Goldschmidt, L.; Teng, P. K.; Riek, R.; Eisenberg, D. Identifying the Amylome, Proteins Capable of Forming Amyloid-like Fibrils. *Proc. Natl. Acad. Sci. U. S. A.* **2010**, *107* (8), 3487–3492. https://doi.org/10.1073/pnas.0915166107.

(63) Phillips, J. C.; Braun, R.; Wang, W.; Gumbart, J.; Tajkhorshid, E.; Villa, E.; Chipot, C.; Skeel, R. D.; Kalé, L.; Schulten, K. Scalable Molecular Dynamics with NAMD. *J. Comput. Chem.* **2005**, *26* (16), 1781–1802. https://doi.org/10.1002/jcc.20289.

(64) Crisafi, F.; Kumar, V.; Perri, A.; Marangoni, M.; Cerullo, G.; Polli, D. Multimodal Nonlinear Microscope Based on a Compact Fiber-Format Laser Source. *Spectrochim. Acta - Part A Mol. Biomol. Spectrosc.* **2018**, *188*, 135–140. https://doi.org/10.1016/j.saa.2017.06.055.

(65) Schindelin, J.; Arganda-Carreras, I.; Frise, E.; Kaynig, V.; Longair, M.; Pietzsch, T.; Preibisch, S.; Rueden, C.; Saalfeld, S.; Schmid, B.; Tinevez, J. Y.; White, D. J.; Hartenstein, V.; Eliceiri, K.; Tomancak, P.; Cardona, A. Fiji: An Open-Source Platform for Biological-Image Analysis. *Nature Methods*. Nature Publishing Group July 28, 2012, pp 676–682. https://doi.org/10.1038/nmeth.2019.

(66) Frigerio, R.; Musicò, A.; Brucale, M.; Ridolfi, A.; Galbiati, S.; Vago, R.; Bergamaschi, G.; Ferretti, A. M.; Chiari, M.; Valle, F.; Gori, A.; Cretich, M. Extracellular Vesicles Analysis in the COVID-19 Era: Insights on Serum Inactivation Protocols towards Downstream Isolation and Analysis. *Cells* **2021**, *10* (3), 544. https://doi.org/10.3390/cells10030544.

TOC graphic:

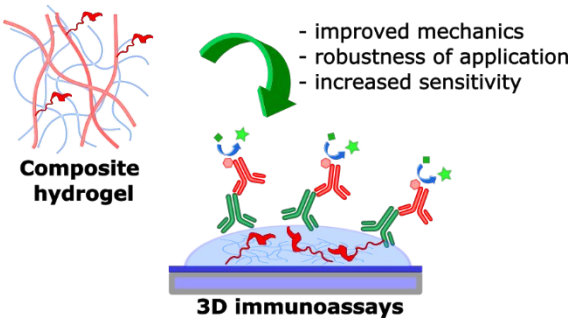
- improved mechanics
- robustness of application
- increased sensitivity
Composite hydrogel
3D immunoassays